HHS Public Access

Author manuscript

J Magn Reson Imaging. Author manuscript; available in PMC 2022 October 01.

Published in final edited form as:

J Magn Reson Imaging. 2021 October ; 54(4): 1053–1065. doi:10.1002/jmri.27638.

Multi-Parametric Evaluation of Cerebral Hemodynamics in Neonatal Piglets using Non-Contrast-Enhanced MRI Methods

Dapeng Liu, PhD[#1,2], **Dengrong Jiang, PhD**[#1], **Aylin Tekes, MD**[1], **Ewa Kulikowicz, MS**[4], **Lee J. Martin, PhD**[3], **Jennifer K. Lee, MD**[4,*], **Peiying Liu, PhD**[1,*], **Qin Qin, PhD**[1,2]

[1]The Russell H. Morgan Department of Radiology and Radiological Science, Johns Hopkins University School of Medicine, Baltimore, Maryland, USA

[2]F.M. Kirby Research Center for Functional Brain Imaging, Kennedy Krieger Institute, Baltimore, Maryland, USA

[3]Department of Pathology, Johns Hopkins University School of Medicine, Baltimore, Maryland, USA

[4]Department of Anesthesiology and Critical Care Medicine, Johns Hopkins University School of Medicine, Baltimore, Maryland, USA

[#] These authors contributed equally to this work.

Abstract

Background: Disruption of brain oxygen delivery and consumption after hypoxic-ischemic injury contributes to neonatal mortality and neurological impairment. Measuring cerebral hemodynamic parameters, including cerebral-blood-flow (CBF), oxygen-extraction-fraction (OEF), and cerebral-metabolic-rate-of-oxygen ($CMRO_2$), is clinically important.

Purpose: Phase-contrast (PC), velocity-selective-arterial-spin-labeling (VSASL) and T_2-relaxation-under-phase-contrast (TRUPC) are MRI techniques that have shown promising results in assessing cerebral hemodynamics in human. We aimed to test their feasibility in quantifying CBF, OEF, and $CMRO_2$ in piglets.

Study Type: Prospective.

Animal Model: Ten neonatal piglets subacutely recovered from global hypoxic-ischemia (n=2), excitotoxic brain injury (n=6), or sham procedure (n=2).

Field Strength/Sequence: VSASL, TRUPC, and PC MRI acquired at 3.0 T.

Assessment: Regional CBF was measured by VSASL. Global CBF was quantified by both PC and VSASL. TRUPC assessed OEF at the superior sagittal sinus (SSS) and internal cerebral veins (ICVs). $CMRO_2$ was calculated from global CBF and SSS-derived OEF. End-tidal carbon dioxide

[*]Corresponding Authors: Peiying Liu (PhD), (peiying.liu@jhu.edu), Department of Radiology, Johns Hopkins University School of Medicine, 600 N. Wolfe St., Park 324, Baltimore, MD, 21287. Jennifer K. Lee, (MD), (jennifer.lee@jhmi.edu), Department of Anesthesiology and Critical Care Medicine, Johns Hopkins University School of Medicine, 1800 Orleans Street, Room 6321, Baltimore, MD 21287.

Financial interests: The authors have nothing to disclose.

($EtCO_2$) levels of the piglets were also measured. Brain damage was assessed in tissue sections postmortem by counting damaged neurons.

Statistical Tests: Spearman correlations were performed to evaluate associations among CBF (by PC or VSASL), OEF, $CMRO_2$, $EtCO_2$ and the pathological neuron counts. Paired t-test was used to compare OEF at SSS with OEF at ICV.

Results: Global CBF was 32.1±14.9 mL/100g/min and 30.9±8.3 mL/100g/min for PC and VSASL, respectively, showing a significant correlation (r=0.82, P<0.05). OEF was 54.9±8.8% at SSS and 46.1±5.6% at ICV, showing a significant difference (P<0.05). Global $CMRO_2$ was 79.1±26.2 μmoL/100g/min and 77.2±12.2 μmoL/100g/min using PC and VSASL-derived CBF, respectively. $EtCO_2$ correlated positively with PC-based CBF (r=0.81, P<0.05) but negatively with OEF at SSS (r=−0.84, P<0.05). Relative CBF of subcortical brain regions and OEF at ICV did not significantly correlate, respectively, with the ratios of degenerating-to-total neurons (P=0.30, P=0.10).

Data Conclusion: Non-contrast MRI can quantify cerebral hemodynamic parameters in normal and brain-injured neonatal piglets.

Keywords

cerebral blood flow; oxygen extraction fraction; cerebral metabolic rate of oxygen; arterial spin labeling; neonatal brain injuries; neuronal cell death

Introduction

Hypoxic-ischemic encephalopathy (HIE) is a leading cause of neonatal mortality and severe neurological impairment in childhood (1). The hypoxic-ischemic (HI) event leads to abnormally reduced cerebral-blood-flow (CBF), and the resulting energy failure can cause cellular death; even if CBF is restored, a multifaceted polymodal secondary energy failure often occurs aggravating brain damage (1). Therefore, measuring CBF, oxygen-extraction-fraction (OEF), and cerebral-metabolic-rate-of-oxygen ($CMRO_2$), the three parameters that characterize cerebral oxidative metabolism, is clinically important. Abnormalities in these hemodynamic parameters have been reported in neonates with HIE compared to normal controls (2–4). However, clinical MRI protocols are not tailored to measure cerebral hemodynamic disturbances in neonates, and it is unclear whether or not HI neuronal damage to neurons, glia, or their subcellular compartments directly relates to these hemodynamic changes. This uncertainty is further complicated by knowledge that these hemodynamic parameters are also affected by other factors such as gestational and postnatal age of the neonate (5,6).

Accurate measurement of CBF and OEF relies on appropriate MRI techniques. Phase-contrast (PC) MRI and arterial-spin-labeling (ASL) have been successfully applied in human neonates to quantify CBF (2–6). PC MRI measures the blood flow in the feeding arteries of the brain to provide a global measurement of CBF and has the advantage of short scan time (1–2 min) (3,5). In contrast, ASL provides regional CBF mapping by magnetically labeling water in the arterial blood as an endogenous tracer (2,4,6). Brain perfusion mapping in healthy and sick newborns have been conducted by both pulsed ASL (PASL) (4,7) and

pseudo-continuous ASL (PCASL) (6,8,9). Compared to PASL, PCASL provides higher sensitivity to perfusion signal and has been demonstrated with better image quality in neonatal brains (8). However, both PASL and PCASL suffer from low signal-to-noise-ratio (SNR) because of the prolonged arterial transit time (ATT) in neonates (9). Alternatively, velocity-selective ASL (VSASL) is insensitive to ATT and has demonstrated improved SNR over conventional ASL methods (10–12).

A limited number of MRI-based techniques have been developed to measure OEF in the human neonatal brain without the use of exogenous contrast agents (2,5,13,14). Among them, T_2-relaxation-under-phase-contrast (TRUPC) is an MRI technique that can measure OEF in multiple major cerebral veins, such as the superior sagittal sinus (SSS) and internal cerebral veins (ICVs), thereby enabling the assessment of OEF for both cortical and subcortical brain regions (14). If OEF and CBF are both quantified, $CMRO_2$ can then be calculated using the Fick principle (5).

Animal models provide the opportunity to develop new metrics to investigate how CBF, OEF, and $CMRO_2$ relate to normal brain structure, function, and brain damage under well controlled conditions. Piglets have similar brain growth patterns and cerebral anatomical structures as human neonates, and the regional distribution of neuropathology in piglet HIE resembles that in human newborns (15). MRI in piglet models of HI and excitotoxicity, an integral cytotoxic molecular cascade that contributes to neonatal HIE (16), can also provide salient information relevant to human neonatal brain injuries (17,18). However, so far, neonatal piglets with brain damage have been primarily interrogated using structural imaging, such as T_1-weighted, T_2-weighted imaging, and diffusion imaging techniques (17,18). There is a paucity of MRI sequences to assess oxygen delivery and consumption in clinically relevant neonatal piglet models of HIE.

To facilitate future investigations on neonatal encephalopathy with the piglet model, we sought to test the feasibility of PC, VSASL and TRUPC in quantifying CBF, OEF, and $CMRO_2$ in different brain regions using piglets recovered from focal excitotoxic or global HI brain injuries.

Materials and Methods

The Animal Care and Use Committee approved all protocols, which were in compliance with the United States Public Health Service Policy on the Humane Care and Use of Laboratory Animals and the Guide for the Care and Use of Laboratory Animals. Ten neonatal male piglets were included. Two encephalopathy models were studied: excitotoxic brain injury model and global HI brain injury model.

Piglet Preparation and Brain Injury Models

Prior to imaging, each piglet underwent one of three procedures: excitotoxic brain injury induced by stereotaxic quinolinic acid (QA) injection into the striatum, global HI injury, or sham procedure. The piglet preparation, procedural anesthesia, and brain injury protocols were previously published (17,18). Briefly, piglets were anesthetized and intubated for mechanical ventilation. The external jugular vein was catheterized for the administration

of fentanyl (20 μg/kg bolus+20 μg/kg/h, intravenous [IV]). A femoral arterial catheter was placed to monitor heart rate and blood pressure. Piglets were kept on warming blankets to maintain normothermia.

Excitotoxic brain injuries were induced in six anesthetized piglets (17,18). Bilateral cranial burr holes 2–3 mm in diameter were drilled 10 mm anterior to the bregma suture and 10–12 mm lateral to midline. A sterile needle was advanced 15 mm deep from the cortical surface to target the putamen, which is an area commonly injured in HIE (19). QA in phosphate-buffered saline (PBS, pH 7.4) was injected into the right brain in different doses: one piglet with 240 nmol (4 μL) injection, three with 720 nmol (12 μL), and two with 960 nmol (16 μL). PBS in equal volume was injected into the left putamen as a control. After QA injection, piglets awakened from anesthesia, recovered for 20 to 96 hours, and then underwent a second anesthetic for MRI as described in the next subsection.

Global HI brain injury was induced in two anesthetized piglets, and an additional two anesthetized piglets underwent sham procedure. To induce hypoxia, the inhaled oxygen concentration was decreased to 10% for 45 minutes. Then the piglets received room air for 5 minutes, which is required for cardiac resuscitation in this model. To cause asphyxia, the endotracheal tube was subsequently clamped for 8 minutes. The piglets were resuscitated with chest compressions, 50% oxygen, and epinephrine 100 μg/kg IV. The sham piglets received the same anesthetic and placement of vascular catheters but without hypoxia or asphyxia. Piglets then recovered from anesthesia and were survived for 45 h to 1 week until the MRI scan.

Anesthesia for MRI

The anesthesia protocol for MRI followed a previously published protocol (17). Immediately before the MRI, the piglets were anaesthetized for tracheostomy. A tracheal tube was placed to bypass potential laryngeal swelling caused by the first intubation. The inhaled anesthetic was titrated off as the piglets were transitioned to propofol (7.5 mg/kg/h IV plus 1–2 mg/kg boluses and infusion increases by 2 mg/kg/h, as-needed) and fentanyl (100 μg/kg/h IV plus 12.5mcg/kg boluses and infusion increases by 12.5 mcg/kg/h, as-needed). To minimize the risk of cerebral hypoperfusion, dopamine was started, when necessary, at 5 mcg/kg/min and titrated to maintain mean arterial blood pressure (MAP) ≥45 mmHg. During the MRI scan, piglets were mechanically ventilated to maintain normocapnia with inhaled 50%/50% oxygen/air. MAP, heart rate, and end-tidal carbon dioxide ($EtCO_2$) were recorded every 15 min. The piglets' hematocrit (Hct) levels were measured prior to the MRI scan.

MRI Sequences

All MRI experiments were performed on a 3 T clinical scanner (Prisma, Siemens Healthineers, Erlangen, Germany) with a 15-channel knee coil.

For structural reference of the piglet brain, a 2D turbo-spin-echo (TSE) T_2-weighted image was acquired with following parameters: repetition time (TR) = 5920 ms; echo time (TE) = 92 ms; slice thickness = 1.2 mm; 42 slices; in-plane resolution = 0.4×0.4 mm^2 with matrix size 256×256; coronal in-plane field of view (FOV) = 100×100

mm^2; GeneRalized-Autocalibrating-Partial-Parallel-Acquisition (GRAPPA) factor = 2; 15 averages; total duration = 15.2 min.

Velocity-selective inversion (VSI) prepared VSASL was implemented with 3D gradient-and-spin-echo (GRASE) readout to obtain cerebral perfusion maps of piglets. The details of the pulse sequence, including the slab-selective saturation module, the VSI label and control modules interleaved through the dynamics, the background suppression and flow-dephasing modules, have been described previously (11). The cutoff velocity for labeling was set as 2.8 cm/s, and the velocity-encoding gradients were applied along the anterior-posterior direction. The delay between slab-selective saturation module and label/control module was 2.5 s. The post-labeling delay (PLD) was chosen as 1.5 s. Parameters for the 3D GRASE readout with coronal orientation were: excitation flip-angle (FA) = 90°; refocusing FA = 120°; acquisition voxel-size = 2.4×2.4×2.4 mm^3 reconstructed to 1.2×1.2×2.4 mm^3; FOV = 158×158×48 mm^3; bandwidth = 2894 Hz/pixel; TE/TR = 17.24/4400 ms; echo-planar-imaging (EPI) factor = 23; TSE factor = 12; four segments were acquired for each image; a total of four label/control pairs for 5 min. A proton density weighted image (SI_{PD}) was also acquired by disabling labeling and setting the TR to 10.0 s (total scan time = 1 min).

To measure PC-based CBF, a time-of-flight (TOF) scan was first performed to visualize the major cerebral feeding arteries, i.e., the left and right internal cerebral arteries (ICAs), using the following parameters: FOV = 120×120×40 mm^3, reconstruction voxel-size = 0.2×0.2×0.5 mm^3, TR/TE = 20.0/3.1 ms, 2 averages, scan time = 2.1 min. Then, two PC scans were acquired to measure the flow through each ICA and were positioned to be perpendicular to each artery based on the TOF scan. The PC sequence parameters included: FOV = 80×80×3 mm^3, voxel-size = 0.3×0.3×3 mm^3, TR/TE = 22.6/7.2 ms, velocity-encoding (VENC) = 10 or 20 cm/s, 6 averages, scan time = 0.6 min.

TRUPC was acquired in a coronal plane approximately 10 mm anterior to the sinus confluence, using the following parameters (14): FOV = 80×80×5 mm^3, acquisition matrix = 160×90, reconstruction voxel-size = 0.5×0.5×5.0 mm^3, VENC = 5 cm/s, TE = 12.3 ms, recovery time = 460 ms, effective echo times (eTEs) = 0, 40, and 80 ms, and scan time = 4.9 min.

Image Processing

The T_2-weighted images were first co-registered to the VSASL images using rigid body transformation with SPM12 (Statistical Parametric Mapping; Wellcome Department of Imaging Neuroscience, Institute of Neurology, London, UK). Data were then analyzed with Matlab 2019b (The MathWorks, Natick, MA, USA) and ImageJ (Rasband W., National Institutes of Health, USA).

VSASL-based CBF maps were calculated using the subtraction of label from control images (ΔS) divided by the equilibrium magnetization of tissue (SI_{PD}) as:

$$\mathrm{CBF} = 6000 \cdot \lambda \cdot \Delta S / \left(2\alpha_{\mathrm{label}} \cdot \alpha_{\mathrm{BGS}} \cdot \mathrm{SI}_{\mathrm{PD}} \cdot e^{-\frac{\mathrm{TE}_{\mathrm{prep}}}{T_{2,\mathrm{tissue}}}} \cdot \mathrm{PLD} \cdot e^{-\frac{\mathrm{PLD}}{T_{1,\mathrm{eff}}}} \right).$$

Here the brain blood partition coefficient, λ, was 0.9 ml/g; α_{label} is the labeling efficiency and α_{BGS} is the correction factor for background suppression, taken as 0.57 and 0.86, respectively, as used in a previous study on adult human brain (11). The duration of the flow dephasing module, TE_{prep}, was 20 ms, and $T_{2,tissue}$ was assumed to be 90 ms. The tissue T_1 of newborn was assumed to be about 1600 ms (20). Since the mean Hct values of piglets were 22.9% (Table 1), the blood T_1 at 3 T was calculated to be 2105 ms based on a Hct-T_1 conversion model (21). Hence $T_{1,eff}$ was taken as 1853 ms, as averaged between tissue T_1 and blood T_1 (11). Finally, CBF units were converted from mL/g/s to mL/100g/min through a factor of 6000.

A neuropathologist and neuroanatomist with 36 years of experience in human and large animal brain (monkey, dog, cat, piglet) neuroanatomy and 20 years of experience in MRI (L.J.M.) and an MRI physicist with 10 years of MRI experience (D.L.) annotated the brain structures on the VSASL-based CBF maps. Regions of interest (ROI) for the whole brain were manually drawn from the final CBF maps (D.L.) to calculate average CBF. For all piglet brains, ROIs were manually drawn in consensus to encompass the left and separately right putamen and caudate. Relative CBF (rCBF) was defined as the ratio of mean CBF of the right ROI to the left ROI.

The PC data were processed following previously reported methods (5). Briefly, the PC sequence produces three images: an anatomic image, a complex difference (CD) image showing the vessels, and a flow velocity map. For each ICA, an ROI was manually drawn by an MRI physicist with 9 years of MRI experience (D.J.) in the CD image by closely tracing the boundary of the artery. This ROI was then applied to the flow velocity map, and the flow rate (in mL/min) of the artery was quantified by spatially integrating the velocities within the ROI. The PC based CBF (mL/100g/min) was calculated by dividing the sum of the flow rates of the two ICAs by the brain mass (in 100g), which was estimated from the volumes of ROIs of the whole brain manually drawn from the high resolution T_2-weighted images (D.L.), assuming a brain tissue density of 1.06 g/mL (5). Note that we did not include the vertebral arteries or the basilar artery in the PC CBF calculation because they were not visible in the TOF angiogram and are very small even in juvenile pigs (22).

The TRUPC images were reconstructed and corrected for eddy-current induced phase errors (14) using in-house Matlab scripts. Two preliminary ROIs were drawn (D.J.) in the CD images to encompass the SSS and ICV, respectively. Within each ROI, the eight pixels with the highest intensities were selected as the final mask. Mono-exponential fitting of the signal intensities inside the final mask was conducted where each pixel was allowed to have individual initial signal but was forced to have the same T_2. Venous oxygenation (Y_v) values were converted from the blood T_2 using a published calibration model (23), based on the measured hematocrit level of each piglet. OEF was then calculated using:

$$OEF = \frac{Y_a - Y_v}{Y_a} \times 100\%$$

assuming an arterial blood oxygenation, Y_a, of 100%. As a metric of the reliability of the OEF value, the width of the 95% confidence interval of $1/T_2$ (ΔR_2) was estimated from the

mono-exponential fitting process. OEF values with $\Delta R_2 \geq 10$ Hz suggested poor data quality and were excluded.

$CMRO_2$ was then calculated as:

$$CMRO_2 = C_{ery} \cdot Hct \cdot Y_a \cdot CBF \cdot OEF$$

where C_{ery} = 21 μmol O_2/mL blood cells (24) and Hct was the measured hematocrit of each piglet. Here the global $CMRO_2$ in units of μmoL/100g/min was derived both from the whole-brain average of VSASL-based CBF maps and the PC-based CBF values separately, with OEF obtained from SSS.

Neuropathology

Neuronal damage was assessed using published method (17,18). Briefly, after the MRI scan, the anesthetized piglets were euthanized and intra-aortically perfused for exsanguination and brain fixation. The heads were submerged in 4% paraformaldehyde for 12–24 hours for further brain fixation. The brain was then removed from the skull and immersed in fresh 4% paraformaldehyde. Finally, the brains were blocked for paraffin processing and sliced into coronal sections (10 μm thick) for hematoxylin and eosin (H&E) staining. H&E tissue sections were identified to anatomically match major structures from the CBF maps by a neuropathologist (L.J.M.) and a MRI physicist (D.L.) in consensus.

One investigator with 10 years of experience in experimental neuropathology (J.K.L.) classified and counted neuronal cell bodies in 9–10 non-overlapping fields in the caudate and 10 non-overlapping fields in the putamen at 400x magnification. Neurons were assigned to one of three categories: 1) normal; 2) degenerating and undergoing irreversible cell death; or 3) injured with uncertain fate and without overt degeneration according to published criteria (17,18). A second investigator with 36 years of neuropathology experience (L.J.M.) screened the slides to verify that two independent observers would reach the same result without any statistically significant differences between the observers' neuron classifications and counts. Both investigators were blinded to the cerebral hemodynamic data and treatment group.

Brain Regional Mitochondrial Localization

We visualized mitochondria within different brain areas to inspect a surrogate histological marker for regional and cellular metabolic demand (27,28). Immunohistochemical staining with a primary antibody for the mitochondrial matrix protein superoxide dismutase 2 (SOD2, 1:100, rabbit polyclonal IgG, Enzo Life Sciences, Farmingdale, NY) was conducted using a published immunoperoxidase protocol (25). The slides were then incubated with goat anti-rabbit IgG (1:20, Sigma Aldrich, St. Louis, MO) secondary antibody and rabbit peroxidase anti-peroxidase soluble complex antibody (1:100, Sigma-Aldrich). Mitochondria were identified as dark brown particles by developing the slides with 3,3′-diaminobenzidine. All slides were stained together for SOD2 immunohistochemistry, and the microscope photographs were taken with the same lighting and imaging software configurations. Post-acquisition image processing for figure construction was identical. Darker brown

staining in different brain regions and cells indicates higher mitochondrial SOD2 density (immunoreactivity).

Statistical analysis

Statistical analyses were performed using Matlab. Results are reported as Mean ± Standard deviation (Std) and coefficient of variation (CoV = Std / Mean) unless otherwise noted. Spearman correlations were used to evaluate the associations: (1) between PC-based global CBF and VSASL-based global CBF averaged from the 3D whole-brain CBF map; (2) between these two global CBF values and the OEF obtained from SSS; (3) between $EtCO_2$ and PC-based global CBF, OEF and $CMRO_2$. The relationships between the deep-brain hemodynamic measures (i.e., right-to-left rCBF in putamen and caudate and OEF measured at ICV) and the neuropathological cell counts (i.e., the ratio of degenerating-, normal-, and injured-to-total neurons in caudate and putamen) were explored using Spearman correlations. Paired t-test was used to compare OEF measured at SSS with OEF measured at ICV. A two-tailed $P < 0.05$ was considered statistically significant. The immunohistochemical data for SOD2 were presented descriptively.

Results

Ten neonatal piglets (2–4 days old, 1–2.2 kg) underwent excitotoxic brain injury from QA (n=6), global HI injury (n=2), or sham procedure (n=2). Sham piglets had highly stable physiological parameters, including arterial pH ~7.4, arterial partial pressure of carbon dioxide ($PaCO_2$) ~ 41 mmHg, arterial partial pressure of oxygen (PaO_2) ~ 140 mmHg, and base excess ~ −3. The physiologic severity of the HI protocol induced similar blood gas physiology at 7 min of asphyxia with arterial pH 6.84 and 6.92, $PaCO_2$ 115 and 108 mmHg, PaO_2 18 and 20 mmHg, and base excess −14.3 and −10.9 in the two piglets. Both piglets were resuscitated with restoration of pH to greater than 7.30, normocarbia, and normoxia and extubated 3 h after the HI injury.

Quantitative regional CBF maps obtained by 3D VSASL from a sham piglet are shown in Figure 1, with corresponding T_2-weighted images. The ROIs of different structures in this sham piglet's brain are delineated in Supporting Information Figure S1. The piglet neocortex showed non-uniform cerebral perfusion with higher CBF in the primary sensory cortical areas (auditory, visual, somatosensory, and olfactory: 41.6±5.2, 39.5±5.7, 33.0±8.5, and 67.7±47.7 mL/100g/min, respectively) (Figure 1, slices 5, 6, 10, 13–16). Primary motor cortex had a CBF of 37.5±6.3 mL/100g/min (Figure 1, slice #7). In contrast, the lateral convexity of the frontal cortex showed lower perfusion (20.7±4.5 mL/100g/min) (Figure 1, slice #1–4). The hippocampus had very low apparent perfusion (12.9±5.1 mL/100g/min) (Figure 1, slice #12). In subcortical forebrain gray matter, the caudate nucleus and putamen (33.2±5.3, 31.7±4.1 mL/100g/min) were divisible from central thalamus and globus pallidus by their higher perfusion (Figure 1, slice #9). Thalamus was also notable because some parts showed low cerebral perfusion while other parts, such as the visual relay lateral geniculate nucleus (LGN) and auditory relay medial geniculate nucleus (MGN), had comparably higher CBF (49.5±6.5, 49.7±6.9 mL/100g/min) (Figure 1, slice #12). The brainstem tectal collicular nuclei visual and auditory relay centers correspondingly showed high CBF

(51.2±39.6 mL/100g/min) (Figure 1, slice #14, 15). Moreover, brainstem structures such as the pons and middle cerebellar peduncle, which are known to provide afferents to cerebellum, were delineated by high perfusion (75.8±21.6 mL/100g/min) (Figure 1, slice #14) in a pattern consistent with high perfusion in the cerebellar vermis (49.7±14.5 mL/100g/min) (Figure 1, slice #17).

Different brain levels seen by H&E staining and SOD2 immunohistochemistry are shown next to the CBF maps. (Figure 2) In a descriptive evaluation of SOD2 immunolocalization, different brain regions appeared distinct because they were divisible by varying intensities of mitochondrial positivity. Figure 2a illustrates this finding with a comparison of high SOD2 immunoreactivity in the LGN (Figure 2a, right) to the much lower SOD2 staining in the nearby hippocampus (Figure 2a, left) within the same tissue section. In brainstem, the superior and inferior colliculi were identifiable in the H&E section and in the CBF map (Figure 2b). Cerebellar cortex showed exquisite distinctions in intracellular mitochondrial loads even within the same cell types but in different cortical subregions. In the lateral cerebellar hemisphere, the neocerebellum, the Purkinje cell bodies were generally SOD2 negative at this age (Figure 2c, left). In the cerebellar vermis, the medial unpaired component of the cerebellar cortex, Purkinje cells had contrastingly high mitochondrial enrichment (Figure 2c, right).

Figure 3 shows two different piglets with 960 nmol QA injection in the right putamen that were scanned ~24 hours after the injury. The T_2-weighted images show the unilateral injury as witnessed by the higher signal intensity (Figure 3a,c, red arrows). Figure 4 shows the TRUPC data of a sham piglet. The physiological values (Hct, $EtCO_2$) and MRI based hemodynamic parameters (CBF, OEF, and $CMRO_2$) of each piglet are listed in Table 1, along with their group-averaged values. One piglet with 960 nmol QA injection was considered as an outlier due to almost twice-of-average $EtCO_2$ and was excluded from the statistical analyses. The Hct and $EtCO_2$ of the remaining nine piglets were 22.9±3.2% and 38.8±4.3 mmHg with CoV of 14.0% and 11.1%, respectively. With the PC-based method, the global CBF was 32.1±14.9 mL/100g/min with a CoV of 46.4%. Using the VSASL-based approach, the CBF averaged from the whole-brain CBF map was 30.9±8.3 mL/100g/min with a CoV of 26.9%. The OEF measured at the SSS was 54.9±8.8% with a CoV of 16.0%. In one piglet, the OEF at ICV was excluded due to $\Delta R_2 \geq 10$ Hz. Across the remaining 8 piglets, OEF at ICV was 46.1±5.6% with a CoV of 12.2% and was significantly lower than the OEF at SSS ($P < 0.05$). With the OEF obtained from SSS, the global $CMRO_2$ derived from PC-measured CBF was 79.1±26.2 μmoL/100g/min with a CoV of 33.1%, and the global $CMRO_2$ derived based on VSASL-measured CBF was 77.2±12.2 μmoL/100g/min with a CoV of 15.8%.

We found a significant positive correlation between PC and VSASL based global CBF values ($N = 7$, $r = 0.82$, $P < 0.05$, Figure 5a). Negative correlations between OEF at SSS and both VSASL global CBF ($N = 8$, $r = -0.88$, $P < 0.05$, Figure 5b) and PC global CBF ($N = 8$, $r = -0.79$, $P < 0.05$, Figure 5c) were observed. $EtCO_2$ was negatively correlated with OEF at SSS ($N = 9$, $r = -0.84$, $P < 0.05$) but positively correlated with PC global CBF ($N = 8$, $r = 0.81$, $P < 0.05$). There was no correlation between $EtCO_2$ and PC-based $CMRO_2$ ($N = 8$, $r = 0.55$, $P = 0.16$) (Figure 5d–f).

For the analysis of neuron counts to MRI, two piglets (one sham and one HI) without neuropathology cell counts were excluded. A third piglet (with QA 720 nmol) was excluded due to imaging artifact in the deep brain CBF map and unreliable OEF at ICV ($\Delta R_2 \geq$ 10Hz). In the remaining six piglets, rCBF of putamen and caudate and OEF obtained from ICV showed no significant correlations with the ratio of degenerating-to-total neurons (rCBF: r = −0.54, P = 0.30, Figure 6a; OEF: r = −0.77, P = 0.10, Figure 6d), the ratio of normal-to-total neurons (rCBF: r = 0.31, P = 0.56, Figure 6b; OEF: r = 0.66, P = 0.17, Figure 6e), or the ratio of injured-to-total neurons (rCBF: r = −0.37, P = 0.50, Figure 6c; OEF: r = −0.49, P = 0.36, Figure 6f).

Discussion

Our study demonstrated the feasibility of multi-parametric evaluation of cerebral hemodynamics in neonatal piglets with excitotoxic and HI brain injury using non-invasive MRI techniques. CBF was evaluated by PC MRI and VSASL, and OEF was evaluated by TRUPC MRI. VSASL provided a high-resolution neuroanatomical interrogation of regional CBF that appears to be related to gray matter mitochondrial enrichment. When averaged across the whole brain, the VSASL-based CBF values of each piglet showed significant correlation with PC based global CBF. $EtCO_2$ was negatively correlated with OEF at SSS. In the striatal areas injured by QA, decreased perfusion signal was revealed in regional CBF maps. We found no significant correlation between neuron counts and rCBF in putamen and caudate or OEF at ICV.

The annotated maps of CBF are salient because they show regional CBF variations in newborn piglet brain within the context of known neuroanatomy. We observed distinct CBF differences in cerebral cortex that match known functional domains. For example, higher perfusion was seen in the primary sensory cortices (olfactory, somatosensory, visual, auditory) compared to the dorsolateral prefrontal cortex. This finding is consistent with advanced maturation in sensory brain regions but not in areas with cognitive and executive functions at this age (26). However, the cingulate cortex also had generally higher CBF than other cortical regions and has executive functions too, but it also has autonomic and limbic functions involved in processing aversive stimuli. The very low perfusion in hippocampus in neonatal piglets reinforces this conclusion. Furthermore, we observed starkly segregated, high perfusion regions within functionally active neural systems and their connectomes. For example, the piglet central visual system, which is an energetically demanding network (27), had high perfusion throughout the brainstem (tectum), diencephalon (LGN), and neocortex (occipital cortex). Thus, mapping CBF in specific brain networks could advance neonatal neurocritical care medicine because metabolism-connectivity could be partially responsible for the neonatal brain’s regional vulnerability to HIE (28). Our observation of relatively higher perfusion to thalami, basal ganglia, brain stem, cerebellum, and sensorimotor cortex than other regions agree with results from applying long or multiple-PLD 3D PCASL in human neonate brain (6,9).

The contrast of perfusion in various brain structures was supported by the localization of mitochondria by SOD2 immunohistochemistry. Visual differences in regional CBF suggest that different structures have varying oxidative phosphorylation needs and that regional

mitochondrial SOD2 differences might distinguish these structures. In prior work (28,29), cytochrome c oxidase enzyme histochemistry was used to map in situ metabolic activity in neonatal piglet brain by disclosing the catalytic activity of complex IV. We could not apply this technique in the current study due to limitations in tissue processing. Notwithstanding, the SOD2 pattern generally matches the mitochondrial activity reported by Martin et al. (29). The perfusion pattern we observed also resembles the reported cerebral glucose metabolism of human newborns using ^{18}F-fluorodeoxyglucose PET (26), reflecting the metabolic activity at the early stages of brain development. The forebrain perfusion was consistent with olfaction being a dominant primary sens in pig (30).

Measuring OEF is traditionally performed by PET imaging with ^{15}O-labeled radiotracers (31). However, the invasive nature of the procedure and exposure to ionizing radiation are major obstacles to its applications in neonates (31). Optical methods such as near infrared spectroscopy (NIRS) have been widely used to monitor neonatal cerebral oxygenation but have difficulty in probing the deep brain structures due to the limited penetration depth of light (32). In the past decade, several MRI-based techniques have been developed to measure OEF on a global level in neonates (2,5,13). However, regional OEF measurement is more desirable because many diseases, such as HIE and stroke, mainly affect specific brain regions (19,33). In this work, we used the TRUPC MRI technique to quantify OEF in two major cerebral veins: the SSS which drains the majority of cerebral cortical veins, the falx cerebri, meninges, diploic veins, and emissary veins; and the ICV which is formed by the unification of the thalamostriatal, septal, and choroidal veins and drains deep brain regions including thalami and basal ganglia. Among them, OEF at SSS has been shown to correlated well with whole-brain averaged OEF measured by ^{15}O-PET (34). We found that $EtCO_2$ correlated positively with PC-based CBF but negatively with OEF at SSS, and there existed a negative correlation between OEF at SSS and CBF (both PC-based and ASL-based). These findings are consistent with previous reports on human adults (35,36) and were thought to be related to the well-known vasodilatory effect of blood CO_2 content and the balance between blood supply and oxygen extraction. We observed a lower OEF at ICV than OEF at SSS, which was consistent with previous reports on human neonates (14). The lower OEF at ICV may be explained by the higher CBF in deep brain structures like thalami and basal ganglia observed in this study and previous literature (6,9).

In our exploratory study of neuropathology in a small sample size, both the rCBF of putamen and caudate and OEF at ICV exhibited negative trends with the ratio of degenerating-to-total neurons; however, none of the associations were statistically significant. Unlike in stroke, piglet models of encephalopathy have selective and regional vulnerability with asynchronous cellular injury and degeneration. Damaged neural cells are not at the same stage of injury at any given time in vivo. To address this, we examined multiple recovery durations to capture different time points after brain injury to better study the neuropathology. We also specifically counted degenerating neurons that were undergoing irreversible, end-stage cell death (17). It should be noted that our neuronal cell counting was conducted in microscope fields that represented a very small portion of the large putamen and caudate ROI that was used to quantify rCBF. Moreover, the ICV-derived OEF included large brain regions that are drained by ICV but were not examined by microscopic

neuropathology, such as the thalami. Therefore, given the small sample size (N=6), it was not surprising that we did not observe significant associations.

Though we did not observe significant relationships between neuron counts and rCBF or OEF, other reports indicate that such a relationship does exist. Using an HI rat model induced by unilateral common carotid artery ligation and subsequent hypoxia, Vannucci et al. found reduced CBF in multiple regions of the ipsilateral cerebral hemisphere and that the extent and spatial distribution of CBF reduction correlated with those of ischemic neuronal necrosis observed in a similar rat model (37). Kurth et al. showed that piglets with longer HI duration tended to have more severe neuronal damage and also a higher cerebral oxygen saturation measured by NIRS, which indicated a lower OEF in these piglets (38). In human neonates, it has also been demonstrated that neonates with HIE had lower OEF than normal controls (2), and neonates with severe HIE had even lower OEF than those with moderate HIE (3). Although the relationships between CBF and/or OEF and neuropathology that we observed were statistically insignificant among a small sample size, our findings may support the rationale for larger studies investigating whether MRI can detect depressed tissue oxygen metabolism with neuronal cell death in neonatal brain.

Medications that induce general anesthesia are known to alter CBF, OEF, and $CMRO_2$. Because all piglets in our study received the same anesthetic regimen, we expect similar anesthesia-related effects on these physiologic parameters in all piglets. Additionally, the inhaled oxygen concentration was closely monitored and maintained at 50% for all piglets during their MRIs scans. We did not study differences in cerebral oxygen supply and demand because that was beyond the scope of our study.

Limitations

Our study had several limitations. For CBF determination, the ROIs were delineated on the perfusion maps rather than from the anatomical maps. This was necessary because CBF maps revealed structural sub-compartmentation better than T2 MRI, including in the LGN and vermis. Our sample size was small, and the mitochondrial and neuropathology aspects of the study were exploratory. The goal of the present study was to test the feasibility of non-invasive quantification of cerebral hemodynamics in newborn piglet models using MRI. Due to the lack of significant correlations between CBF or OEF and the pathological neuron counts, it is out of the scope of this study to determine which hemodynamic parameter (CBF, OEF or $CMRO_2$) has better sensitivity to brain injuries. Nonetheless, future studies with larger sample size are needed to fully investigate the association of CBF and OEF with mitochondrial localization and neuropathology, and compare the sensitivities to brain injury among the hemodynamic parameters. The TRUPC OEF measurements focused on large veins, i.e., SSS and ICVs, which receive venous blood drainage from large territories in both hemispheres, and due to the limited image resolution, we could not separate the left and right ICVs. These factors reduced the sensitivity of our OEF measurements to injuries induced by unilateral QA injection. Regional OEF measurement techniques that can measure OEF in smaller veins or even provide voxel-wise OEF mapping (39,40) will have better sensitivity and specificity to brain diseases and injuries that mainly affect specific regions. Therefore, future technical development of the TRUPC technique should target

on imaging smaller cortical or subcortical veins that are closer to the injury sites. The piglets also had a delay between the acute brain injury and MRI scanning, which renders the observations temporally out of phase. In this regard, real-time MRI interrogation of excitotoxic lesion evolution would be novel and useful in providing needed insight into early sentinel mechanisms and neural consequences of stroke.

Conclusion

We measured hemodynamic parameters (CBF, OEF and $CMRO_2$) in neonatal piglet brain using non-contrast MRI techniques. VSASL-based CBF maps revealed well-defined regional CBF patterns that corresponded to known functional domains and matched to brain regions with varying mitochondrial enrichments as seen by direct localization of these organelles. CBF and OEF relationships to neuropathology were inconclusive. Our results suggest that these methods may be useful for monitoring perfusion and oxygenation of brain development and neuropathological conditions in human neonates.

Supplementary Material

Refer to Web version on PubMed Central for supplementary material.

Grant support:

National Institutes of Health R01 NS109029 (to P.L.), R01 HL144751 (to Q.Q.), R01 NS107417 (to J.K.L. and L.J.M.), and R01 NS113921 (to J.K.L. and L.J.M.).

References

1. Allen KA, Brandon DH. Hypoxic Ischemic Encephalopathy: Pathophysiology and Experimental Treatments. Newborn Infant Nurs Rev2011;11:125–133. [PubMed: 21927583]
2. De Vis JB, Petersen ET, Alderliesten T, et al.Non-invasive MRI measurements of venous oxygenation, oxygen extraction fraction and oxygen consumption in neonates. Neuroimage2014;95:185–192. [PubMed: 24685437]
3. Shetty AN, Lucke AM, Liu P, et al.Cerebral oxygen metabolism during and after therapeutic hypothermia in neonatal hypoxic-ischemic encephalopathy: a feasibility study using magnetic resonance imaging. Pediatr Radiol2018.
4. Proisy M, Corouge I, Legouhy A, et al.Changes in brain perfusion in successive arterial spin labeling MRI scans in neonates with hypoxic-ischemic encephalopathy. NeuroImage: Clinical2019;24:101939. [PubMed: 31362150]
5. Liu P, Huang H, Rollins N, et al.Quantitative assessment of global cerebral metabolic rate of oxygen (CMRO2) in neonates using MRI. NMR Biomed2014;27:332–340. [PubMed: 24399806]
6. Ouyang MH, Liu PY, Jeon T, et al.Heterogeneous increases of regional cerebral blood flow during preterm brain development: Preliminary assessment with pseudo-continuous arterial spin labeled perfusion MRI. Neuroimage2017;147:233–242. [PubMed: 27988320]
7. De Vis JB, Hendrikse J, Petersen ET, et al.Arterial spin-labelling perfusion MRI and outcome in neonates with hypoxic-ischemic encephalopathy. Eur Radiol2015;25:113–121. [PubMed: 25097129]
8. Boudes E, Gilbert G, Leppert IR, et al.Measurement of brain perfusion in newborns: Pulsed arterial spin labeling (PASL) versus pseudo-continuous arterial spin labeling (pCASL). Neuroimage-Clin2014;6:126–133. [PubMed: 25379424]

9. Kim HG, Lee JH, Choi JW, Han M, Gho SM, Moon Y. Multidelay Arterial Spin-Labeling MRI in Neonates and Infants: Cerebral Perfusion Changes during Brain Maturation. Am J Neuroradiol2018;39:1912–1918. [PubMed: 30213808]
10. Qin Q, van Zijl PC. Velocity-selective-inversion prepared arterial spin labeling. Magn Reson Med2016;76:1136–1148. [PubMed: 26507471]
11. Liu D, Xu F, Li W, van Zijl PC, Lin DD, Qin Q. Improved velocity-selective-inversion arterial spin labeling for cerebral blood flow mapping with 3D acquisition. Magn Reson Med2020;84:2512–2522. [PubMed: 32406137]
12. Bolar DS, Gagoski B, Orbach DB, et al.Comparison of CBF Measured with Combined Velocity-Selective Arterial Spin-Labeling and Pulsed Arterial Spin-Labeling to Blood Flow Patterns Assessed by Conventional Angiography in Pediatric Moyamoya. AJNR Am J Neuroradiol2019;40:1842–1849. [PubMed: 31694821]
13. Jain V, Buckley EM, Licht DJ, et al.Cerebral oxygen metabolism in neonates with congenital heart disease quantified by MRI and optics. J Cereb Blood Flow Metab2014;34:380–388. [PubMed: 24326385]
14. Jiang D, Lu H, Parkinson C, et al.Vessel-specific quantification of neonatal cerebral venous oxygenation. Magn Reson Med2019;82:1129–1139. [PubMed: 31066104]
15. Koehler RC, Yang ZJ, Lee JK, Martin LJ. Perinatal hypoxic-ischemic brain injury in large animal models: Relevance to human neonatal encephalopathy. J Cereb Blood Flow Metab2018;38:2092–2111. [PubMed: 30149778]
16. Johnston MV. Excitotoxicity in perinatal brain injury. Brain Pathol2005;15:234–240. [PubMed: 16196390]
17. Lee JK, Liu D, Raven EP, et al.Mean Diffusivity in Striatum Correlates With Acute Neuronal Death but Not Lesser Neuronal Injury in a Pilot Study of Neonatal Piglets With Encephalopathy. J Magn Reson Imaging2020;52:1216–1226. [PubMed: 32396711]
18. Lee JK, Liu D, Jiang D, et al.Fractional anisotropy from diffusion tensor imaging correlates with acute astrocyte and myelin swelling in neonatal swine models of excitotoxic and hypoxic-ischemic brain injury. J Comp Neurol2021.
19. Shankaran S, Barnes PD, Hintz SR, et al.Brain injury following trial of hypothermia for neonatal hypoxic-ischaemic encephalopathy. Arch Dis Child Fetal Neonatal Ed2012;97:F398–404. [PubMed: 23080477]
20. Dubois J, Alison M, Counsell SJ, Lucie HP, Huppi PS, Benders MJNL. MRI of the Neonatal Brain: A Review of Methodological Challenges and Neuroscientific Advances. J Magn Reson Imaging2020.
21. Li W, Grgac K, Huang A, Yadav N, Qin Q, van Zijl PC. Quantitative theory for the longitudinal relaxation time of blood water. Magn Reson Med2016;76:270–281. [PubMed: 26285144]
22. Ssali T, Anazodo UC, Thiessen JD, Prato FS, St Lawrence K. A Noninvasive Method for Quantifying Cerebral Blood Flow by Hybrid PET/MRI. J Nucl Med2018;59:1329–1334. [PubMed: 29523628]
23. Lu H, Xu F, Grgac K, Liu P, Qin Q, van Zijl P. Calibration and validation of TRUST MRI for the estimation of cerebral blood oxygenation. Magn Reson Med2012;67:42–49. [PubMed: 21590721]
24. Xu F, Li W, Liu P, et al.Accounting for the role of hematocrit in between-subject variations of MRI-derived baseline cerebral hemodynamic parameters and functional BOLD responses. Hum Brain Mapp2018;39:344–353. [PubMed: 29024300]
25. Lee JK, Santos PT, Chen MW, et al.Combining Hypothermia and Oleuropein Subacutely Protects Subcortical White Matter in a Swine Model of Neonatal Hypoxic-Ischemic Encephalopathy. J Neuropathol Exp Neurol2020.
26. Chugani HT. A critical period of brain development: Studies of cerebral glucose utilization with PET. Prev Med1998;27:184–188. [PubMed: 9578992]
27. Wong-Riley MT. Energy metabolism of the visual system. Eye Brain2010;2:99–116. [PubMed: 23226947]
28. Martin LJ, Brambrink A, Koehler RC, Traystman RJ. Primary sensory and forebrain motor systems in the newborn brain are preferentially damaged by hypoxia-ischemia. J Comp Neurol1997;377:262–285. [PubMed: 8986885]

29. Martin LJ, Brambrink AM, Price AC, et al.Neuronal death in newborn striatum after hypoxia-ischemia is necrosis and evolves with oxidative stress. Neurobiol Dis2000;7:169–191. [PubMed: 10860783]

30. Morrow-Tesch J, McGlone JJ. Sources of maternal odors and the development of odor preferences in baby pigs. J Anim Sci1990;68:3563–3571. [PubMed: 2262409]

31. Altman DI, Perlman JM, Volpe JJ, Powers WJ. Cerebral oxygen metabolism in newborns. Pediatrics1993;92:99–104. [PubMed: 8516092]

32. Dehaes M, Aggarwal A, Lin PY, et al.Cerebral oxygen metabolism in neonatal hypoxic ischemic encephalopathy during and after therapeutic hypothermia. J Cereb Blood Flow Metab2014;34:87–94. [PubMed: 24064492]

33. De Vis JB, Petersen ET, Kersbergen KJ, et al.Evaluation of perinatal arterial ischemic stroke using noninvasive arterial spin labeling perfusion MRI. Pediatr Res2013;74:307–313. [PubMed: 23797533]

34. Jiang D, Deng S, Franklin CG, et al.Validation of T2 -based oxygen extraction fraction measurement with (15) O positron emission tomography. Magn Reson Med2020.

35. Jiang D, Lin Z, Liu P, et al.Normal variations in brain oxygen extraction fraction are partly attributed to differences in end-tidal CO2. J Cereb Blood Flow Metab2020;40:1492–1500. [PubMed: 31382788]

36. Ibaraki M, Shinohara Y, Nakamura K, Miura S, Kinoshita F, Kinoshita T. Interindividual variations of cerebral blood flow, oxygen delivery, and metabolism in relation to hemoglobin concentration measured by positron emission tomography in humans. J Cereb Blood Flow Metab2010;30:1296–1305. [PubMed: 20160738]

37. Vannucci RC, Lyons DT, Vasta F. Regional cerebral blood flow during hypoxia-ischemia in immature rats. Stroke; a journal of cerebral circulation1988;19:245–250.

38. Kurth CD, McCann JC, Wu J, Miles L, Loepke AW. Cerebral oxygen saturation-time threshold for hypoxic-ischemic injury in piglets. Anesth Analg2009;108:1268–1277. [PubMed: 19299799]

39. Fan AP, Bilgic B, Gagnon L, et al.Quantitative oxygenation venography from MRI phase. Magn Reson Med2014;72:149–159. [PubMed: 24006229]

40. Christen T, Bolar DS, Zaharchuk G. Imaging brain oxygenation with MRI using blood oxygenation approaches: methods, validation, and clinical applications. AJNR Am J Neuroradiol2013;34:1113–1123. [PubMed: 22859287]

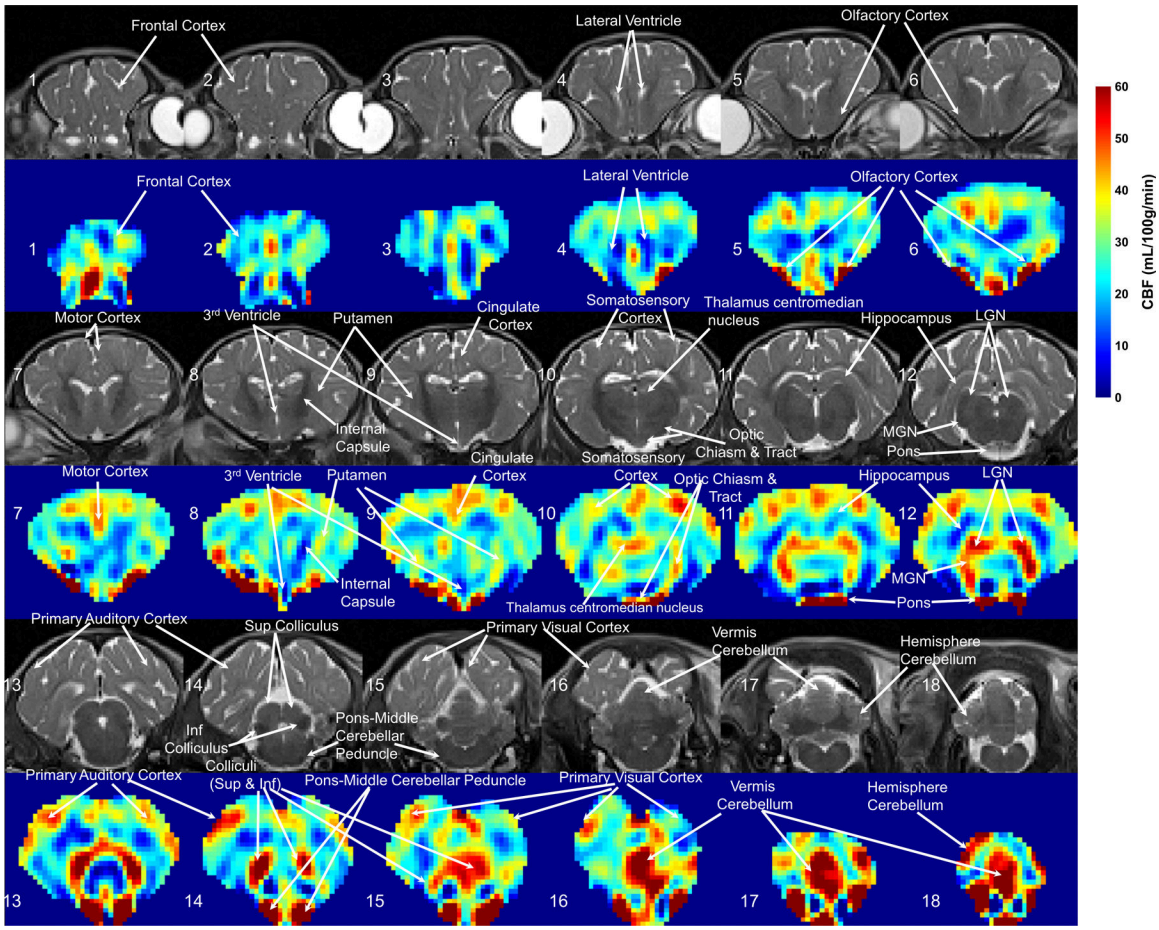

Figure 1:

Representative cerebral blood flow (CBF) maps derived from VSASL with 3D acquisition and whole–brain coverage from an anesthetized neonatal piglet after a sham procedure. The co-registered T_2-weighted structural images are placed above the corresponding CBF maps. Coronal images are displayed and slice numbers are labeled from anterior (#1, top left) to posterior (#18, bottom right). Various brain structures and anatomical landmarks are annotated. Higher CBF values (see scale at right), indicating the areas where the metabolic activities are most active at this stage of postnatal development, were observed in the olfactory cortex (#5,6), somatosensory cortex (#10), motor cortex (#7), cingulate cortex (#9), dorsal thalamus (#12), including the lateral geniculate nucleus (LGN) and medial geniculate nucleus (MGN), brainstem (#14,15), including the tectum, and vermis cerebellum (#17).

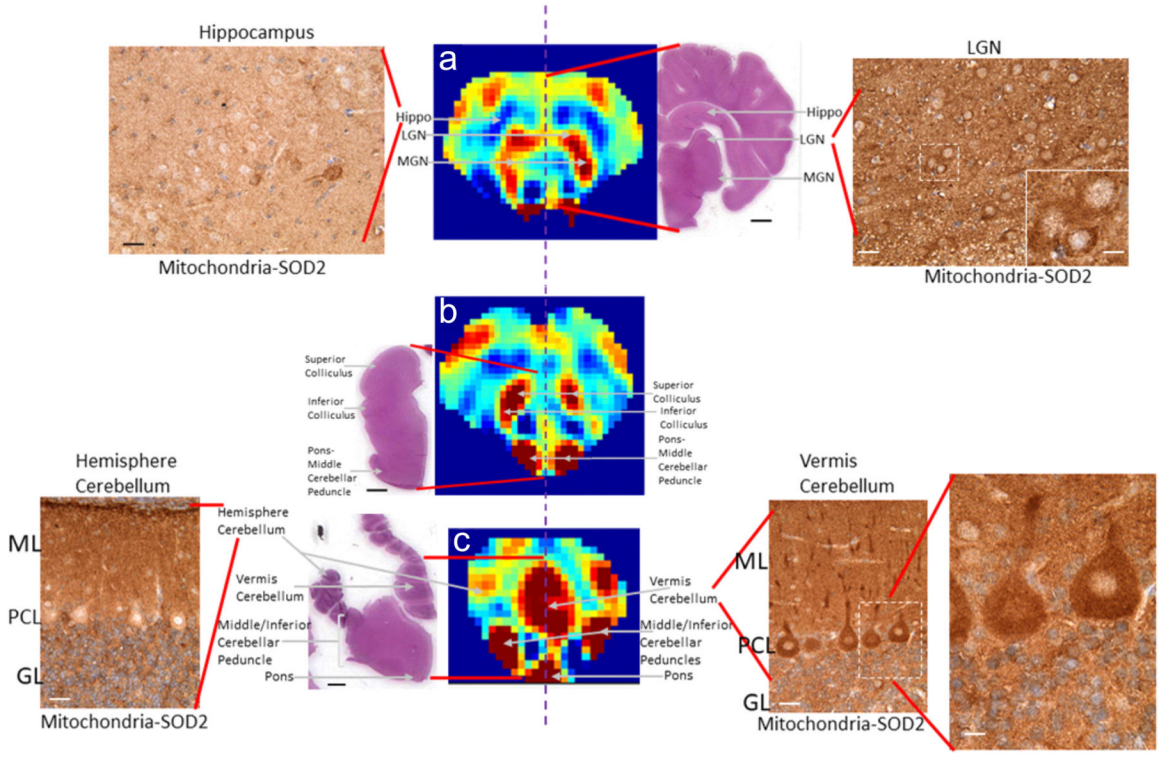

Figure 2:

Slices #12, #14, and #17 (top to bottom) of the VSASL-based CBF maps of the piglet brain shown in Figure 1 with anatomically matched histological brain sections immunohistochemically stained for the mitochondrial matrix marker superoxide dismutase 2 (SOD2) at corresponding diencephalic (a), midbrain tectum (b), and medulla-cerebellum (c) levels. Hatched vertical lines identify the midline. Perfusion maps at each level are paired with a hematoxylin and eosin (H&E)-stained hemibrain sections to show the neuroanatomy of each level. (a) At the diencephalic level, the lateral geniculate nucleus (LGN) and medial geniculate nucleus (MGN) in thalamus have high perfusion, while the overlying hippocampus has low perfusion. The LGN (right) shows greater mitochondrial SOD2 staining, seen as brown punctate particles (inset), with higher mitochondrial enrichment than in hippocampus (left). (b) At the midbrain tectum level, the superior and inferior colliculi and pons-middle cerebellar tract have high perfusion. The overall surface contour of the tissue section appears different from the corresponding CBF map because the overlying occipital lobe has detached and is not present in the tissue sections because of the transverse fissure. (c) At the medulla-cerebellum level, the pontine nuclei, middle cerebellar peduncles, and cerebellar vermis have high perfusion whereas the lateral cerebellar hemisphere has lower perfusion. The cerebellar cortical vermis (right) has high mitochondrial SOD2 localization (brown signal), including in the molecular layer (ML), Purkinje cell layer (PCL), and the granule cell layer (GL). The enlarged inset shows Purkinje cell bodies and dendrites that are highly enriched in mitochondria (brown particles). In contrast, the lateral cerebellar hemisphere (left) has notably lower mitochondria density. The contour of the tissue section appears different from the CBF map due to the absence of the occipital lobe in the section. Scale bars in the H&E images are (a) 4.2 mm, (b) 3 mm, (c) 5 mm. All slides

were simultaneously stained for SOD2 immunohistochemistry. Microscope photographs were taken in the same lighting. Darker brown staining indicates greater mitochondrial SOD2 density (immunoreactivity). Scale bars in the SOD2 immunohistochemistry panels are 16 μm, and the inset bars are 8 μm.

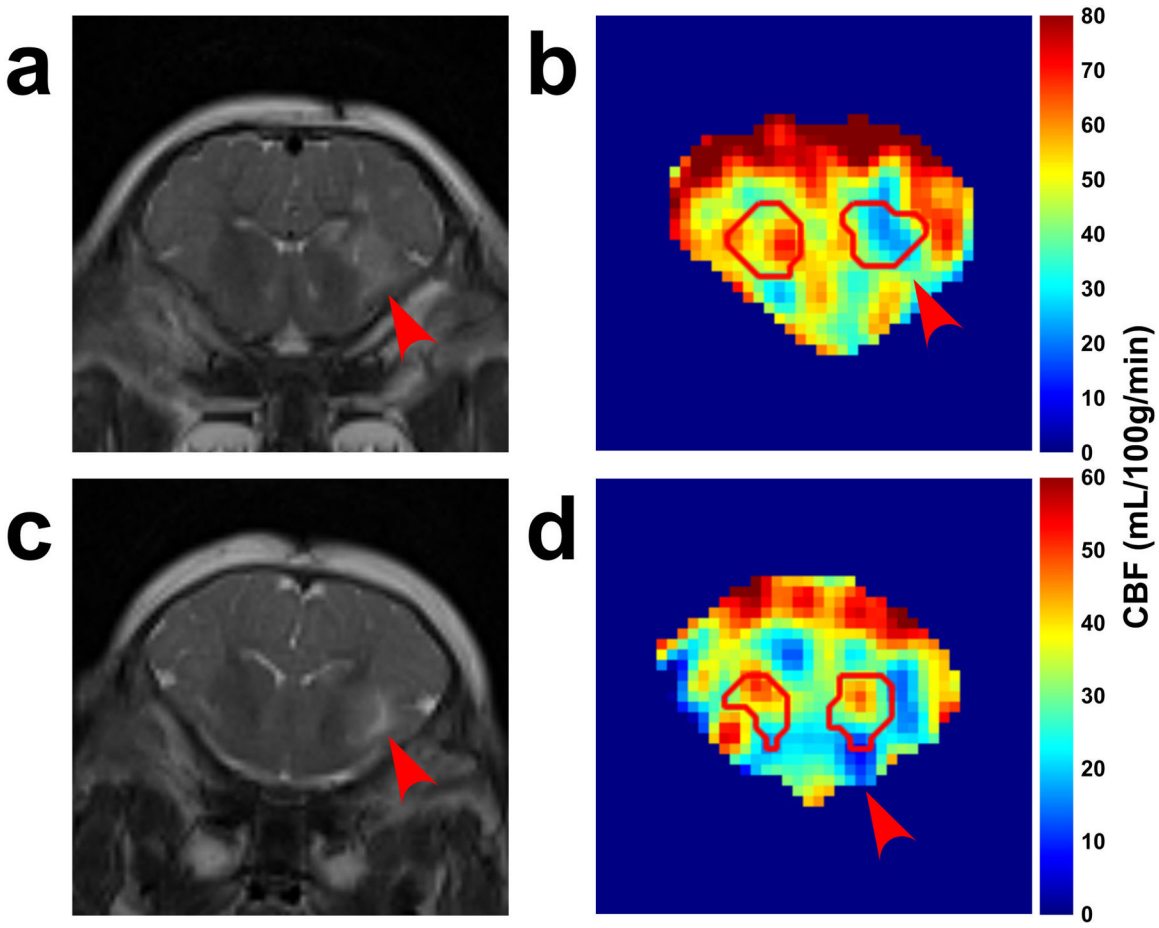

Figure 3:

Representative MR images from two piglets (a,b: piglet #7; c,d: piglet #8) that received stereotaxic injections of quinolinic acid (QA, 960 nmol) and contralateral phosphate-buffered saline (PBS, control). (a,c) T_2-weighted images show higher T_2 signal in the putamen and caudate on the side that received QA (red arrows) compared to the contralateral control side. (b,d) cerebral blood flow (CBF) maps with manually defined ROIs containing the putamen and caudate show decreased signal in the regions injured by QA (red arrows).

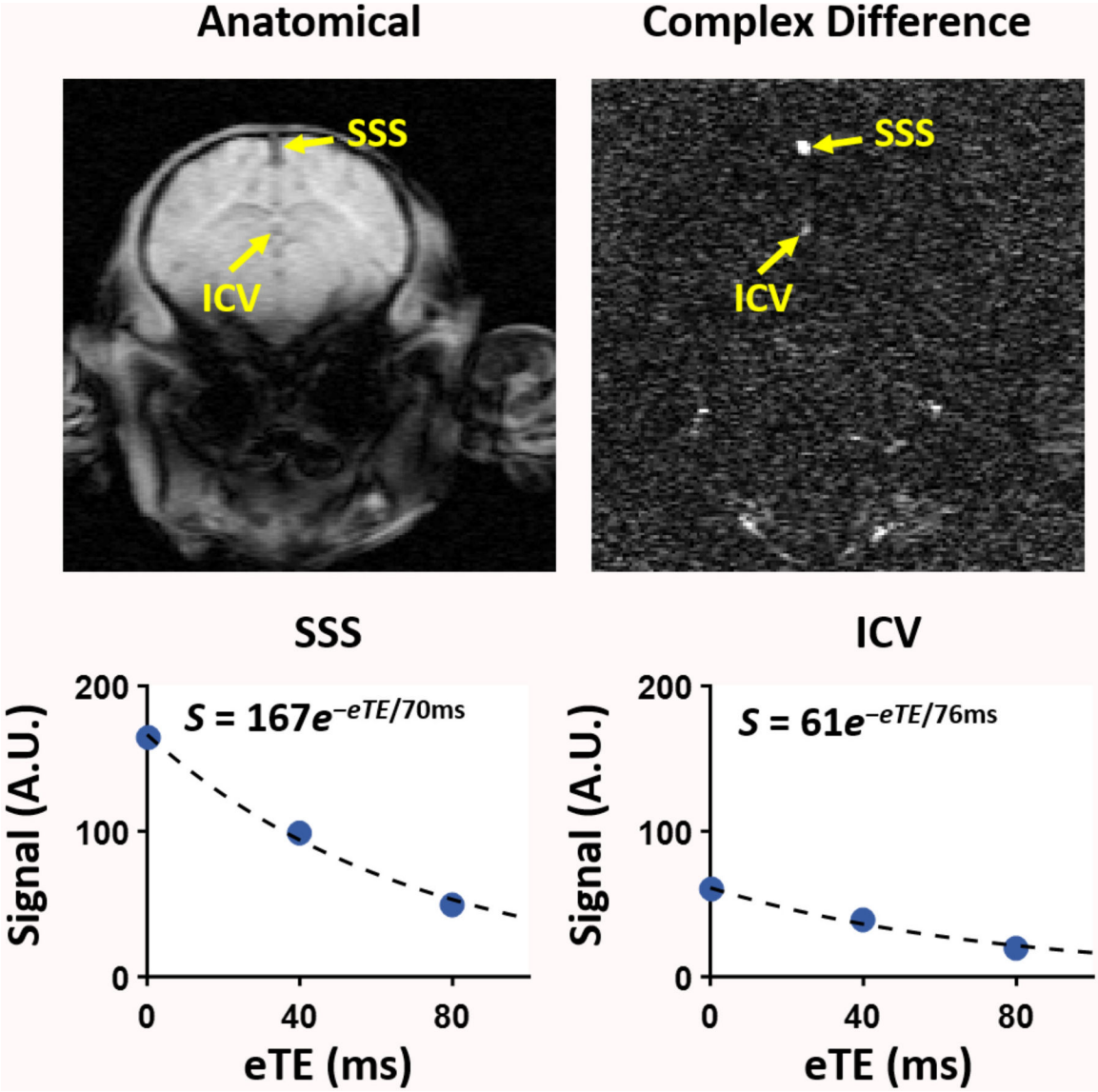

Figure 4:

Data from T_2-relaxation-under-phase-contrast (TRUPC) of a representative piglet for estimating oxygen extraction fraction (OEF). Venous signals in the superior sagittal sinus (SSS) and internal cerebral vein (ICV) can be seen in the complex difference image, although the ICV signal has a relatively lower SNR. The scatter plots at the bottom show the averaged venous blood signals as a function of effective TEs (eTEs) for SSS and ICV, respectively. The solid curves indicate the fitted results. The fitted equations are also shown.

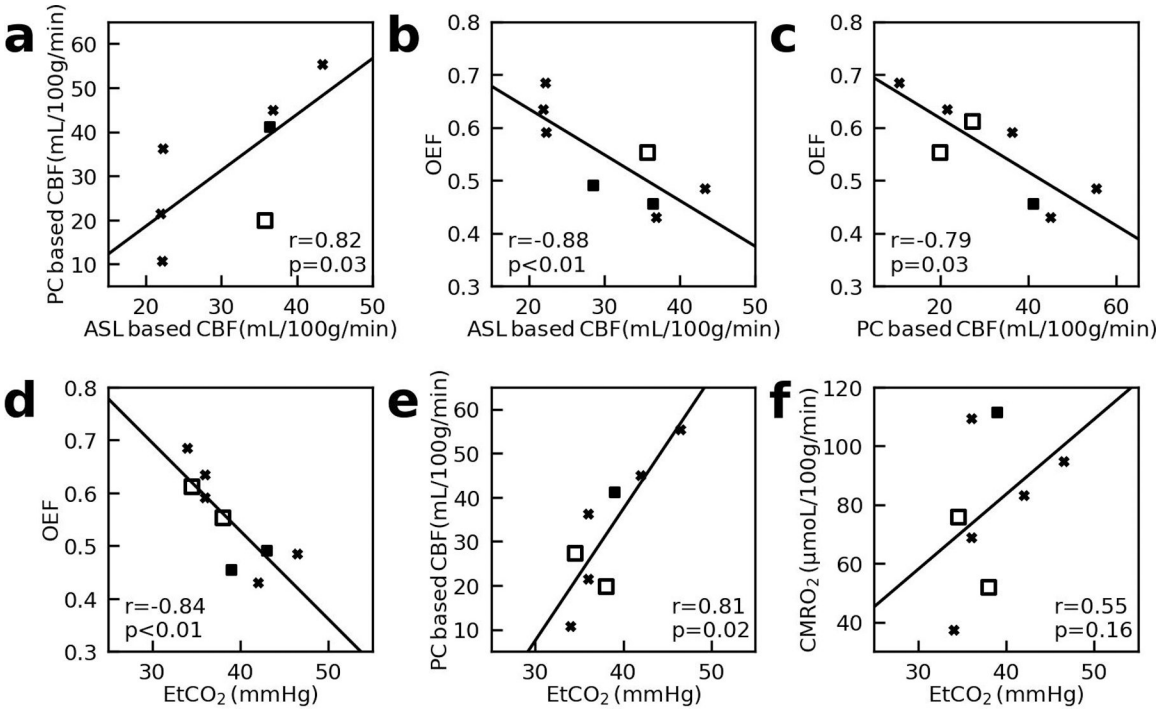

Figure 5:

Correlations between (a) phase-contrast (PC) based global cerebral-blood-flow (CBF) and velocity-selective-arterial-spin-labeling (VSASL) based averaged CBF values; (b) oxygen-extraction-fraction (OEF) and VSASL-based CBF; (c) OEF and PC-based CBF; (d) OEF and end-tidal carbon dioxide ($EtCO_2$); (e) PC-based CBF and $EtCO_2$; (f) cerebral-metabolic-rate-of-oxygen of the whole brain ($CMRO_2$) and $EtCO_2$. Here OEF were obtained from superior sagittal sinus (SSS). X-marks indicate piglets with quinolinic acid-induced brain injury. Solid squares indicate piglets with global hypoxic-ischemic brain injury. The open square represents a piglet that underwent the sham procedure. The lines of best-fit are also shown.

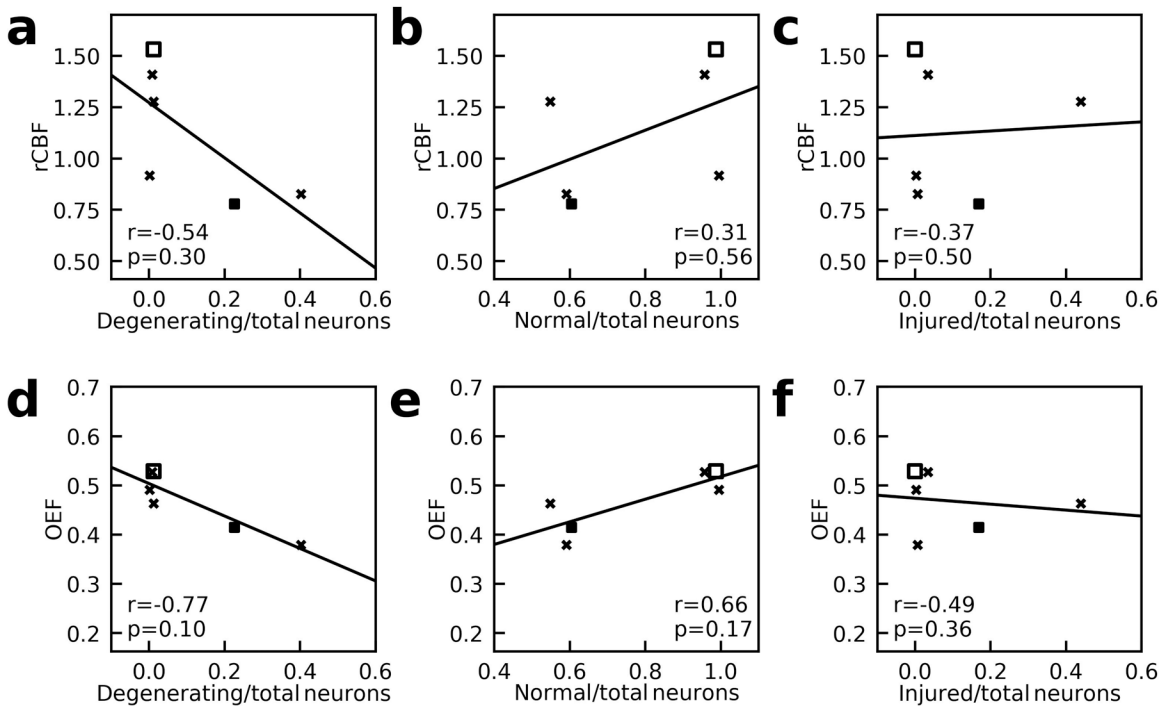

Figure 6:

Correlation between (a) the relative CBF (rCBF) of putamen and caudate of right side to the left side and the ratio of degenerating-to-total neurons; (b) rCBF and the ratio of normal-to-total neurons; (c) rCBF and the ratio of injured-to-total neurons; (d) oxygen-extraction-fraction (OEF) and the ratio of degenerating-to-total neurons; (e) OEF and the ratio of normal-to-total neurons; (f) OEF and the ratio of injured-to-total neurons. Here OEF values were obtained from the ICV. X-marks indicate piglets with quinolinic acid-induced brain injury. Solid squares indicate piglets with global hypoxic-ischemic brain injury. The open square represents a piglet that underwent the sham procedure. The lines of best-fit are also shown.

Table 1:

Physiological and hemodynamic parameters of each piglet.

piglet #	Treatment	Time after injury (hour)	Hct (%)	$EtCO_2$ (mmHg)	TRUPC		PC		VSASL		
					OEF (ICV) (%)	OEF (SSS) (%)	CBF (ml/min/ 100g)	$CMRO_2$ (μ mol/min/ 100g)	rCBF	CBF (ml/min/ 100g)	$CMRO_2$ (μ mol/min/ 100g)
1	Sham	168	21.6	34.5	48.1	61.2	27.3	75.9	N/A	N/A	N/A
2	Sham	23	22.5	38.0	52.8	55.4	19.9	51.9	1.5	35.7	93.3
3	QA (240 nmol)	96	24.1	36.0	46.3	63.4	21.5	68.9	1.3	21.9	70.3
4	QA (720 nmol)	96	24.3	34.0	N/A	68.5	10.7	37.4	N/A	22.2	77.4
5	QA (720 nmol)	91	24.3	36.0	52.7	59.1	36.3	109.4	1.4	22.2	67.1
6	QA (720 nmol)	20	16.8	46.5	49.1	48.5	55.4	94.8	0.9	43.3	74.2
7	QA (960 nmol)	25	23.4	77.5	21.2	21.3	279.3	292.3	0.7	64.4	67.4
8	QA (960 nmol)	24	20.4	42.0	37.9	43.1	45.0	83.1	0.8	36.8	68.0
9	HI	45	23.4	43.0	41.4	49.1	N/A	N/A	0.8	28.5	68.8
10	HI	65	28.4	39.0	40.5	45.5	41.1	111.5	0.9	36.4	98.7
Mean			22.9	38.8	46.1	54.9	32.1	79.1	1.1	30.9	77.2
Std			3.2	4.3	5.6	8.8	14.9	26.2	0.3	8.3	12.2
CoV (Std/Mean, %)			14.0	11.1	12.2	16.0	46.4	33.1	28.3	26.9	15.8

QA: quinolinic acid injection; HI: global hypoxia-ischemia; Hct: hematocrit; $EtCO_2$: end-tidal carbon dioxide; TRUPC: T_2-relaxation-under-phase-contrast; PC: phase contrast; VSASL: velocity-selective arterial spin labeling; OEF: oxygen extraction fraction; SSS: superior sagittal sinus; ICV: internal cerebral vein; CBF: global cerebral-blood-flow for PC or whole-brain averaged CBF for VSASL; rCBF is the relative CBF of putamen and caudate of right side to the left side; $CMRO_2$: cerebral metabolic rate of oxygen of the whole brain; Std: standard deviation; CoV: coefficient of variation; N/A: data not acquired. Piglet #7 was considered as an outlier due to almost twice-of-average $EtCO_2$, and excluded from the statistical analyses.